Understanding the saturation state of argon in the thermocline: The role of air-sea gas exchange and diapycnal mixing

T. Ito[1] and C. Deutsch[2]

Received 14 November 2005; revised 30 March 2006; accepted 10 April 2006; published 7 September 2006.

[1] Using a hierarchy of models, we develop a theoretical framework for understanding the physical processes controlling the magnitude and patterns of the saturation state of dissolved argon (δAr) in the ocean. A conceptual box model of the argon cycle demonstrates that the saturation state of argon in the thermocline can be considered a linear combination of a preformed disequilibrium (δAr_{pre}) governed by surface processes and mapped into the ocean interior, and a supersaturation driven by diapycnal mixing in the interior ocean (δAr_{mix}). The magnitude of δAr_{mix} is determined by the relative strength of isopycnal ventilation and diapycnal mixing in the thermocline. We extend the simple theory to a three-dimensional, continuously stratified ocean by deriving a mathematical relationship between diapycnal mixing, air-sea heat fluxes and the saturation state of argon. This relationship predicts that the δAr of a water parcel increases following its flow path at a rate that is proportional to the diapycnal diffusivity (κ). The theoretical predictions are evaluated with a numerical ocean basin model showing reasonable agreement between simulated argon distribution and the theory. We find three distinctive regimes in which different dynamical balances determine the saturation state of argon in the thermocline. First, newly ventilated water in the subtropical gyre is dominated by δAr_{pre}, reflecting the balance between air-sea heat transfer and the gas exchange rates. Second, the saturation state of argon in the tropical thermocline is primarily determined by δAr_{mix}, reflecting the important roles of diapycnal mixing there. Third, at the transition between the ventilated gyre and the poorly ventilated tropics, δAr_{pre} and δAr_{mix} together control the saturation state of argon. In this region, δAr is sensitive to model diffusivity, which can be estimated from the simulated distribution of δAr with an error of less than 50%. Thus noble gas concentrations may provide a unique constraint on the basin-scale diapycnal diffusivity of the subtropical thermocline.

Citation: Ito, T., and C. Deutsch (2006), Understanding the saturation state of argon in the thermocline: The role of air-sea gas exchange and diapycnal mixing, *Global Biogeochem. Cycles*, *20*, GB3019, doi:10.1029/2005GB002655.

1. Introduction

[2] The distribution of dissolved gases in the ocean provides a wealth of information about physical and biological oceanic processes that play an important role in the climate system. Gleaning mechanistic insights from tracer distributions poses a formidable challenge, however, especially for biologically active gases such as CO_2 or O_2 that are influenced by a complex interplay of air-sea gas exchange, biological cycling, and physical transport. Inert gases not affected by biology have proven useful tracers of physical ocean processes alone, but can be difficult to interpret owing to complex atmospheric histories [*Fuchs et al.*, 1987; *Warner et al.*, 1996]. Perhaps the simplest are the noble gases, which have no internal oceanic sources or sinks and a constant atmospheric burden, yielding steady state distributions that are determined solely by air-sea gas exchange and ocean transport.

[3] Noble gases have been widely used as tracers of local air-sea gas exchange processes [*Emerson et al.*, 1995; *Battle et al.*, 2003]. More recently, modeling studies have shown Ar in the ocean interior to be sensitive to diapycnal mixing [*Henning et al.*, 2006]. While the large-scale distributions of the noble gases are currently poorly known, recent analytical advances allow several noble gases to be more accurately and widely sampled [*Emerson et al.*, 1999; *Hamme and Emerson*, 2004b]. Here we explore the types of insights that might be gained from a more complete characterization of the large-scale distributions of noble gases in the ocean.

[1] Joint Institute for the Study of the Atmosphere and Ocean, University of Washington, Seattle, Washington, USA.
[2] Program on Climate Change, School of Oceanography, University of Washington, Seattle, Washington, USA.

0886-6236/06/2005GB002655$12.00

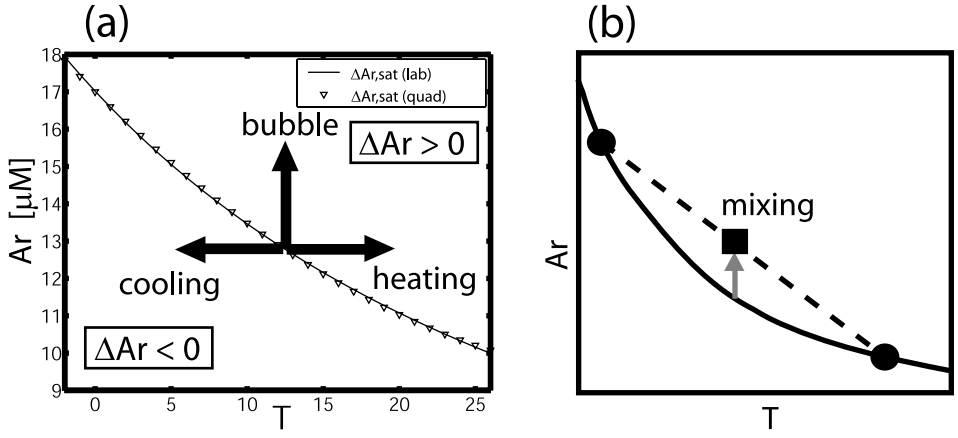

Figure 1. Argon solubility as a function of temperature, with processes capable of producing a disequilibrium (a) in surface waters and (b) in the interior. Solid line in Figure 1a is based on the solubility of *Hamme and Emerson* [2004a], and triangles are the quadratic approximation as described in equation (2). In Figure 1a, surface heating and bubble injection lead to supersaturation, while cooling causes undersaturation. In Figure 1b, mixing of two saturated water masses (solid circles) produces temperature and Ar values along a conservative mixing line (solid square on dashed line) which lies above the Ar saturation line (solid line, curvature exaggerated for clarity). The vertical distance between the mixing and solubility curves reveals the mixing-induced supersaturation.

We present a simple quantitative theory for the combined roles of ocean mixing, ventilation, and air-sea gas exchange that aims to address the following questions: (1) How do air-sea gas exchange, ocean ventilation and mixing combine to determine the distribution of the saturation state of oceanic Ar? (2) Can we distinguish the effects of gas exchange and diapycnal mixing on Ar distributions? (3) How sensitive is the Ar distribution to ocean ventilation and mixing? (4) Might Ar provide a constraint on the rates of ocean mixing? Although we have chosen to focus on a single gas, Argon (Ar), the theory developed here will apply quite generally to any of the noble gases, whose solubilities are qualitatively similar.

[4] The solubility of Ar in seawater is a decreasing function of both temperature and salinity, so that the saturated Ar concentration, Ar_{sat}, is greater in cold/fresh waters than in warm/salty waters. The experimentally determined magnitude of Ar_{sat} varies by 50% over the full range of oceanic temperatures but only 2–3% over the range of oceanic salinity [*Hamme and Emerson*, 2004a]. The saturation state of Ar is commonly expressed as

$$\Delta Ar = \frac{\delta Ar}{Ar_{sat}} \times 100(\%), \qquad (1)$$

where $\delta Ar = Ar - Ar_{sat}$ is the difference between measured and saturated Ar concentrations. Supersaturations (undersaturations) are represented by positive (negative) values of both δAr and its normalized value, ΔAr.

[5] Oceanic Ar concentrations are observed to be within a few percent of their saturated values [*Hamme and Emerson*, 2002] indicating that the temperature dependence of Ar solubility exerts the primary influence on the oceanic Ar distribution. Processes that decouple Ar from temperature to produce Ar disequilibria with coherent spatial structure are, however, of greatest interest. We discuss these in turn.

[6] In the surface ocean mixed layer, where both the heat and Ar content can be changed through interaction with the atmosphere, several processes are able to produce Ar disequilibria. First, because the solubility of Ar is a decreasing function of temperature, heating or cooling of a water parcel alters its Ar solubility (Figure 1a). Heating decreases Ar_{sat}, driving the surface water toward supersaturation ($Ar_{sat} <$ Ar), while cooling tends to produce undersaturation ($Ar_{sat} >$ Ar). The magnitude of the resulting Ar disequilibrium will depend on the degree to which Ar can also be exchanged across the air-sea interface in response that disequilibrium.

[7] In the absence of heating or cooling, Ar can also be transferred from the atmosphere to the ocean by the injection of air bubbles. Breaking surface waves generate small air bubbles which, under elevated hydrostatic pressure, can increase the transfer of dissolved gases into the surrounding water [e.g., *Keeling*, 1993]. Changes in total atmospheric pressure can similarly produce an air-sea Ar disequilibrium.

[8] Once a surface water parcel is isolated from the atmosphere through subduction or sinking, its Ar concentration is conserved. Any disequilibrium obtained at the surface will be carried into the ocean interior along the pathways of water mass transport. We will therefore refer to any Ar disequilibrium in the ocean interior whose origin can be traced back to the surface layer as a "preformed" Ar disequilibrium.

[9] In contrast to the concentration of Ar, its saturation state (δAr) is not a conservative tracer in the interior ocean owing to the nonlinear temperature dependence of argon solubility [*Bieri et al.*, 1966]. The mixing of saturated water parcels, which affects both temperature and argon linearly, will have an Ar concentration that is supersaturated with

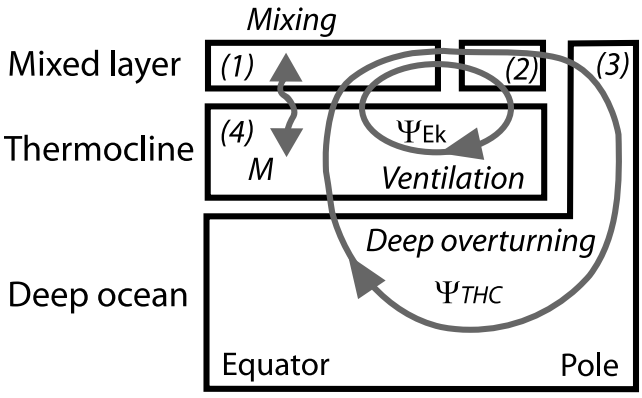

Figure 2. Schematic depiction of the four-box model.

respect to the temperature of the mixture (Figure 1b). Because mixing of water parcels with different temperatures raises the saturation state of Ar, δAr is a potential tracer of ocean mixing that occurs across isotherms. Recent modeling studies demonstrate that this mechanism significantly impacts the modeled argon saturation [*Henning et al.*, 2006].

[10] The distribution of ΔAr therefore consists of both a preformed value, determined through air-sea gas exchange and transported into the interior, and a second component due to mixing. In section 2, we describe how these processes combine to set the large-scale pattern of ΔAr in a highly idealized box model. The ideas developed in the box-model framework are then extended to a three-dimensional ocean by deriving a relationship between ocean diffusivity and δAr. We test these theoretical relationships in section 3, using an Ocean General Circulation Model, showing that basin scale diffusivity can be estimated from distributions of Ar and temperature with an error of less than 50%. The sensitivity of ΔAr to diapycnal mixing is examined in section 4, followed by a summary of how Ar can provide new insights into biogeochemically and climatically important ocean processes.

2. Theory

[11] Here we develop a simple theory describing how air-sea gas exchange and mixing combine to determine the saturation state of Ar and its sensitivity to key physical processes in different ocean regions. To accomplish this, we begin with a highly idealized box model (Figure 2) that is designed to include simple representations of processes most relevant to the large-scale Ar distribution.

[12] The surface ocean is divided into three regions; low latitudes (box 1), middle latitudes (box 2), and high latitudes (box 3). Properties of the deep ocean are determined by high-latitude surface waters and are therefore also represented by box 3. The thermocline (box 4) is at intermediate depths between the surface and deep ocean boxes. Its properties are governed by several idealized physical processes. First, a "thermohaline" meridional overturning circulation Ψ_{THC}, which ventilates the deep ocean from high latitudes and upwells into the low-latitude surface ocean through the thermocline. Second, a wind-driven, shallow meridional overturning circulation, Ψ_{EK}, represents ventilation of the thermocline due to Ekman pumping at midlatitudes. Finally, bidirectional water fluxes, M, are included to represent diapycnal mixing between warm surface waters and thermocline waters (see Table 1 for a list of physical parameters used in this box model).

[13] We first discuss physical aspects of the box model with relevance for Ar (section 2.1), and then examine solutions for ΔAr. We treat the effect of air-sea gas exchange and diapycnal mixing separately for conceptual understanding in sections 2.2 and 2.3, respectively. These processes are considered in combination in section 2.4, allowing their influences on ΔAr to be distinguished. Finally, we extend the results of the box model to a three-dimensional ocean in section 2.5.

[14] In deriving the relationships that follow, we make use of the linear quantity, δAr, although the numerical results will be presented in terms of the normalized value, ΔAr. In addition, we approximate the solubility curve as a quadratic function of temperature (Figure 1a).

$$Ar_{sat}(T) = a_0 + a_1\,T + a_2\,T^2. \tag{2}$$

For suitable coefficients (a_0 = 16.9 μM, a_1 = −0.398 μM deg^{-1}, and a_2 = 5.17 × 10^{-3} μM deg^{-2}) we find that a quadratic T dependence is a very good approximation to the more complicated solubility function [*Hamme and Emerson*, 2004a].

2.1. Physical Solutions

[15] Anticipating the importance of heating and cooling for the saturation state of argon at the sea surface, we begin by examining the relationship between air-sea heat flux and transport parameters in the box model. A simple heat budget requires that at steady state, air-sea heat fluxes balance the divergence of meridional heat transport,

$$\mathcal{H}_1 = \frac{\rho\, c_p}{A_1}(\Psi_{EK}\Delta T_{12} + \Psi_{THC}\Delta T_{13}), \tag{3}$$

$$\mathcal{H}_2 = \frac{\rho\, c_p}{A_2}(\Psi_{EK} + \Psi_{THC})\Delta T_{21}, \tag{4}$$

$$\mathcal{H}_3 = \frac{\rho\, c_p}{A_3}\Psi_{THC}\Delta T_{32}, \tag{5}$$

where $\mathcal{H}_i$ represents air-sea heat flux for the ith box (positive into the ocean), A_i is its surface area, and ρ and c_p

Table 1. Physical Parameters Used in the Box Model

Model Parameter	Symbol	Units	Value
Ventilation rate	Ψ_{EK}	S_V	6.0
Mixing rate	M	S_V	0–5
Gas transfer coeff	G	ms^{-1}	2.0 × 10^{-5}
Low lat. area	A_1	m^2	2.8 × 10^{13}
Middle lat. area	A_2	m^2	6.0 × 10^{12}
High lat. area	A_3	m^2	2.0 × 10^{12}
Low lat. temp	T_1	°C	25
Middle lat. temp	T_2	°C	15
High lat. temp	T_3	°C	0

are the density and specific heat of seawater. Temperature differences between the ith and jth box are defined as $\Delta T_{ij} = T_i - T_j$. Thus a stronger overturning circulation (Ψ_{EK} or Ψ_{THC}) or a stronger meridional temperature gradient (i.e., ΔT_{ij}) is associated with greater heat transport divergence (i.e., terms of the form $\Psi \Delta T_{ij}$) requiring a greater rate of heat loss at middle and high latitudes and stronger heat uptake at low latitudes. Because air-sea heat flux is determined by the divergence of horizontal heat transport, it does not directly depend on vertical mixing.

[16] The temperature of surface waters, together with the mass fluxes, also determines the temperature of the thermocline box, which is a flux-weighted average of surface end-member temperatures,

$$T_4 = \frac{M\,T_1 + \Psi_{EK}\,T_2 + \Psi_{THC}\,T_3}{M + \Psi_{EK} + \Psi_{THC}}. \tag{6}$$

In order to focus on properties along an isopycnal surface, we consider the solution in which the temperature of the thermocline box is equal to the middle latitude "outcrop" (i.e., $T_4 = T_2$). Having specified the vertical stratification at low latitudes (via T_4), the rate of thermohaline overturning is linked to the vertical mixing rate at low latitudes,

$$\Psi_{THC} = \frac{\Delta T_{12}}{\Delta T_{23}}\,M, \tag{7}$$

which is equivalent to a well-known result in physical oceanography [*Munk*, 1966]. We now see that although vertical mixing is not an explicit factor in the heat fluxes (see equations (3)–(5)), stronger mixing is associated with enhanced ocean heat transport and air-sea heat flux, through its impact on the "thermohaline" overturning circulation.

[17] Because mixing of waters with different temperatures will tend to produce Ar supersaturation, we now describe the composition of thermocline water in terms of the relative abundance, or mixing ratio, of each of the three surface end-members. The mixing ratios, f_i, of the three surface end-members are equal to the respective temperature coefficients in equation (6). They can be related to surface temperatures and mass fluxes by combining equations (6) and (7),

$$(f_1, f_2, f_3) = \left(\left(\frac{\Delta T_{13}}{\Delta T_{23}} + \gamma \right)^{-1}, 1 - \frac{\Delta T_{13}}{\Delta T_{23}} f_1, \frac{\Delta T_{12}}{\Delta T_{23}} f_1 \right), \tag{8}$$

where the dimensionless parameter, $\gamma = \dfrac{\Psi_{EK}}{M}$, is a measure of the relative importance of ventilation versus mixing. When vertical mixing is rapid relative to advective ventilation ($\gamma \rightarrow 0$), thermocline properties are determined by the mixture of the low-latitude and high-latitude surface end-members with little influence from midlatitudes ($f_2 \rightarrow 0$ and $f_1 + f_3 \rightarrow 1$). In contrast, when horizontal ventilation is rapid relative to vertical mixing ($\gamma \rightarrow \infty$), thermocline waters reflect primarily the preformed properties from the midlatitude outcrop ($f_2 \rightarrow 1$) with little influence from deep or low-latitude surface waters ($f_1, f_3 \rightarrow 0$). Thus the mixing ratio of low-latitude surface waters, f_1, provides a measure of the relative importance of mixing and ventilation in setting thermocline stratification.

2.2. ΔAr and Air-Sea Gas Exchange

[18] An important component of the δAr distribution is formed in surface waters by incomplete equilibration of Ar concentrations between the ocean and atmosphere. The air-sea flux of Ar, F_{Ar}, may result from both a diffusive flux, F_D, and a bubble-mediated flux, F_B,

$$F_{Ar} = F_D + F_B. \tag{9}$$

For diffusive gas exchange, the air-sea Ar flux is related to its disequilibrium through a mass transfer coefficient (piston velocity), G, so that $F_D = -G\,\delta Ar$.

[19] A second, independent equation for the total air-sea Ar flux holds when air-sea gas exchange is relatively fast with respect to the ocean transport timescales. In this case the air-sea flux of Ar, F_{Ar}, is locally coupled to the air-sea heat flux, $\mathcal{H}$,

$$F_{Ar} = \frac{\mathcal{H}}{\rho\,c_p} \frac{\partial Ar_{sat}}{\partial T}. \tag{10}$$

(See section 2.5 for a detailed derivation.) Combining these equations allows surface δAr to be written as

$$\delta Ar = -\frac{\mathcal{H}}{\rho\,c_p\,G} \frac{\partial Ar_{sat}}{\partial T} + \frac{F_B}{G}, \tag{11}$$

revealing that surface δAr is proportional to both the heat flux, $\mathcal{H}$, and to the bubble-injection, F_B, but inversely related to the piston velocity, G. Gas transfer due to bubbles is poorly understood, and for the sake of simplicity we neglect F_B in the remainder of this study.

[20] Assuming that F_B is small compared to diffusive gas exchange, box model solutions for δAr at the surface (Figure 3b) are immediately obtained by combining air-sea heat fluxes (equations (3)–(5)) and the relationship between $\mathcal{H}$ and δAr (equation (11)). The low-latitude surface box is supersaturated in Ar owing to local net heating, whereas undersaturation prevails at middle and high latitudes due to net heat loss. The magnitude of surface Ar disequilibria is ultimately determined by the balance between the heat transport, $\Psi \Delta T$, and the area-weighted piston velocity, $A_i G$. Stronger heat transport increases the surface Ar disequilibrium, while faster gas exchange (either through wide surface area or rapid air-sea gas transfer) brings surface water toward saturation.

[21] Neglecting the effect of mixing on the saturation state of Ar, the thermocline δAr is a linear combination of surface δAr values,

$$\delta Ar_{4,pre} = f_1 \delta Ar_1 + f_2 \delta Ar_2 + f_3 \delta Ar_3. \tag{12}$$

The notation, $\delta Ar_{4,pre}$, signifies that the argon saturation in the thermocline box is caused solely by the surface disequilibrium. As the rate of vertical mixing increases, preformed ΔAr in the thermocline (Figure 4) experiences

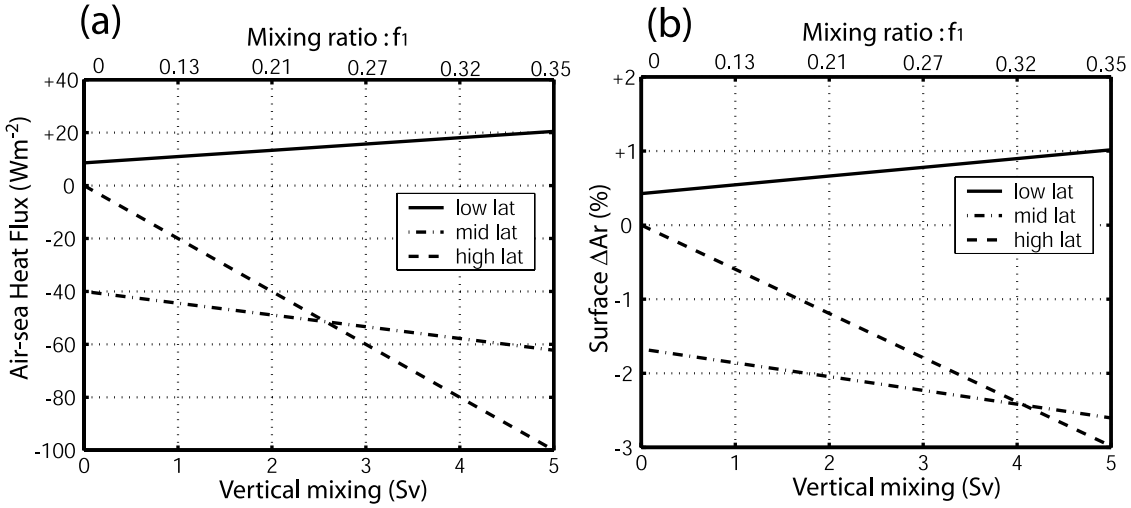

Figure 3. Box model solutions for (a) surface heat flux and (b) surface argon disequilibrium as a function of mixing rate, M (lower x axis), or equivalently, the mixing ratio of low-latitude surface waters in the thermocline box, f_1 (upper x axis).

two competing effects. First, the influence of supersaturated low-latitude surface waters (i.e., f_1) increases, causing preformed thermocline δAr to rise. Second, the increase in mixing enhances high-latitude cooling, causing the deep ocean and its contribution to preformed thermocline δAr to become more undersaturated. The influence of these two effects largely cancel each other, so that ΔAr_{pre} in the thermocline box remains negative (approximately −2%) across a wide range of vertical mixing rates.

2.3. ΔAr and Diapycnal Mixing

[22] Owing to the nonlinear dependence of Ar_{sat} on temperature, the mixing of water parcels with different temperatures can increase thermocline ΔAr above its preformed value. Here we consider a simple case where air-sea gas exchange is fast enough to maintain surface waters near thermodynamic equilibrium, so that Ar has no preformed disequilibrium ($\delta Ar_1 = \delta Ar_2 = \delta Ar_3 = 0$), allowing us to focus on the mixing component of δAr in isolation. The Ar concentration in the thermocline box is then a mixture of saturated surface end-members,

$$Ar_4 = f_1 Ar_{sat}(T_1) + f_2 Ar_{sat}(T_2) + f_3 Ar_{sat}(T_3). \quad (13)$$

The saturation state in the thermocline box is determined from

$$\delta Ar_{4,mix} = Ar_4 - Ar_{sat}(T_4), \quad (14)$$

where the notation, $\delta Ar_{4,mix}$, signifies that the argon saturation is driven solely by vertical mixing. Combining equations (2), (8), (13), and (14) we find

$$\delta Ar_{4,mix} = a_2 f_1 \Delta T_{12} \Delta T_{13}. \quad (15)$$

The mixing component of δAr in the thermocline is therefore a product of the curvature of Ar solubility, a_2, the mixing ratio of low latitude surface waters, f_1, and the temperature gradients between surface and deep water (ΔT_{13}), and between surface and thermocline ($\Delta T_{12} = \Delta T_{14}$), both measures of vertical stratification.

[23] The simple, linear relationship between δAr_{mix} and f_1 reveals that it is the relative strength of diapycnal mixing versus advective ventilation that governs the mixing component of Ar supersaturation. The mixing component of thermocline δAr decreases linearly with f_1, approaching zero in the limit where horizontal ventilation is dominant ($f_1 \rightarrow 0$) (Figure 4). While we have assumed here that

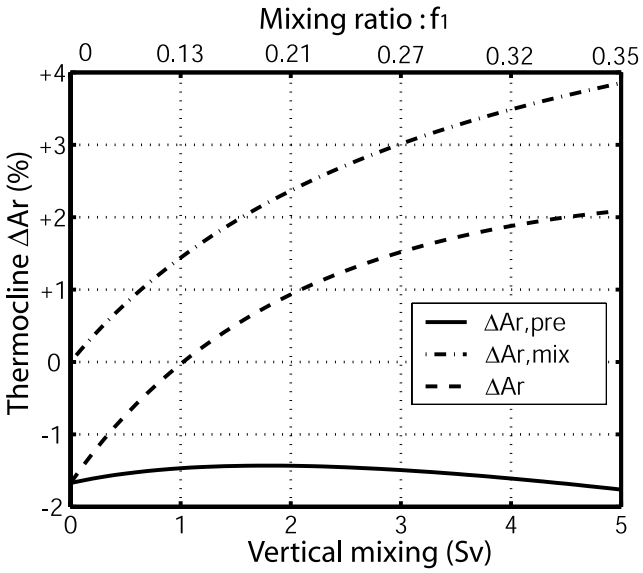

Figure 4. Box model solutions for thermocline ΔAr (dashed line) and its preformed (solid line) and mixing (dash-dotted line) components, as a function of mixing rate (M, horizontal axis).

surface Ar is in equilibrium, the fundamental concept does not depend on this assumption, which will be relaxed below, as we consider mixing and gas-exchange effects together.

2.4. Superposition and Separation of ΔAr

[24] Here we consider the net effect of gas exchange and mixing acting simultaneously on the distribution of δAr. Most generally, thermocline Ar depends on the mixing ratio and Ar concentration of surface end-members,

$$Ar_4 = f_1\,Ar_1 + f_2\,Ar_2 + f_3\,Ar_3. \tag{16}$$

In surface waters, any Ar disequilibrium is by definition preformed, so that $Ar = Ar_{sat} + \delta Ar_{pre}$. Taking the difference between Ar_4 and $Ar_{sat}(T_4)$, and using the definition of $\delta Ar_{4,pre}$ and $\delta Ar_{4,mix}$ from equations (12) and (14), we find

$$\delta Ar_4 = \delta Ar_{4,pre} + \delta Ar_{4,mix}, \tag{17}$$

which shows that δAr in the thermocline is simply the sum of two components: the preformed and mixing-induced disequilibria (Figure 4, dashed line). When vertical mixing is weak and stratification is maintained by advective ventilation, argon is undersaturated in the thermocline. As vertical mixing becomes stronger, argon saturation increases toward supersaturation owing to the rapid increase in $\delta Ar_{4,mix}$.

[25] In the real ocean, the individual components of δAr are not directly measurable and the observed argon saturation reflects the sum of $\delta Ar_{4,pre}$ and $\delta Ar_{4,mix}$. However, we can approximate the partitioning between the two components applying the box model theory (see Appendix A for detailed derivation),

$$\delta Ar_{4,mix} = \frac{\delta Ar_4 - \delta Ar_2}{\left(\sum_{i=1}^{3} c_i \delta Ar_i\right) + 1}, \tag{18}$$

where $c_1^{-1} = a_2\Delta T_{12}\Delta T_{13}$, $c_2^{-1} = a_2\Delta T_{21}\Delta T_{23}$ and $c_3^{-1} = a_2\Delta T_{31}\Delta T_{32}$. Thus, given the Ar concentration in the thermocline, the mixing and preformed components of ΔAr can be separately determined, provided the end-member values for T and Ar are known.

[26] To summarize, four conclusions can be drawn from the simple box model. (1) Saturation state of Ar in the thermocline is the sum of two components, a preformed disequilibrium obtained at the surface and mapped into the ocean interior, δAr_{pre}, and a component due to mixing across isotherms within the interior, δAr_{mix} (equation (17)). (2) Saturation state of Ar in the surface waters is controlled by the balance between air-sea heat flux and area-integrated gas exchange rates (equation (11)). (3) Mixing component of Ar saturation in the thermocline box reflects the relative importance of vertical mixing versus advective ventilation, and is linearly proportional to the mixing ratio of the low latitude end-member, f_1 (equation (15)). (4) Combining the temperature and Ar concentration of surface end-members, we can infer the partitioning of in situ Ar saturation between δAr_{pre} and δAr_{mix} in the thermocline (equation (18)).

2.5. Extension to a Stratified Three-Dimensional Ocean

[27] The saturation state of Ar in the thermocline reservoir of the box model has been shown to depend on the relative importance of diapycnal mixing and advective ventilation. In reality, different regions of the oceanic thermocline may reflect different physical balances between these processes. Here we derive a continuity equation for the saturation state of Ar, and formulate some scaling relationships which generalize the simple box model theory in the context of a continuously stratified, three-dimensional ocean.

[28] We use the "residual mean" formulation [*Andrews and McIntyre*, 1976; *Marshall*, 1997; *Ito et al.*, 2004] to write the governing equations for the large-scale distribution of temperature and argon,

$$\frac{\partial T}{\partial t} + \mathbf{u_{res}} \cdot \nabla T = \frac{\partial}{\partial z}\left(\kappa \frac{\partial T}{\partial z}\right) + \frac{\mathcal{H}}{\rho\, c_p\, h} \tag{19}$$

$$\frac{\partial Ar}{\partial t} + \mathbf{u_{res}} \cdot \nabla Ar = \nabla \cdot \mathbf{K} \nabla Ar + \frac{\partial}{\partial z}\left(\kappa \frac{\partial Ar}{\partial z}\right) + \frac{F_{Ar}}{h}, \tag{20}$$

where F_{Ar} is the air-sea flux of argon (see section 2.2), and h is the thickness of the surface mixed layer. The "residual mean" flow, $\mathbf{u_{res}}$, is the sum of an Eulerian mean circulation and the advective transport by mesoscale eddies. Furthermore, argon is stirred along isopycnals by mesoscale eddies, as represented by the first term on the RHS of equation (20).

[29] The governing equation for δAr can be derived (see Appendix B for details) using the quadratic approximation of Ar_{sat} (equation (2)),

$$\frac{\partial \delta Ar}{\partial t} + \mathbf{u_{res}} \cdot \nabla \delta Ar = \nabla \cdot \mathbf{K} \nabla \delta Ar + \frac{\partial}{\partial z}\left(\kappa \frac{\partial \delta Ar}{\partial z}\right) + \left(\frac{\partial^2 Ar_{sat}}{\partial T^2}\right)\kappa\left(\frac{\partial T}{\partial z}\right)^2 - \left(\frac{\partial Ar_{sat}}{\partial T}\right)\frac{\mathcal{H}}{\rho\, c_p\, h} + \frac{F_{Ar}}{h}. \tag{21}$$

[30] The first four terms in equation (21) represent the time rate of change, advection, and isopycnal and diapycnal diffusion of the Ar disequilibrium, δAr. The last two terms are due to air-sea interaction and describe the dominant balance in the mixed layer. Equating these two terms leads to the approximation for our previous air-sea Ar flux (equation (10)), which can now be seen to hold regardless of the mechanisms of gas exchange.

[31] The third term on the RHS of equation (21) represents an internal source of δAr due to diapycnal mixing. Through this term, the effect of vertical diffusion on the distributions of temperature and Ar concentrations acts to increase δAr locally at the rate of $(\frac{\partial^2 Ar_{sat}}{\partial T^2})\,\kappa\,(\frac{\partial T}{\partial z})^2$. We will refer to this term as the saturation production rate (hereinafter SPR). The existence of the positive definite source makes δAr fundamentally different from other tracers, in that vertical diffusion locally increases δAr while simultaneously redistributing δAr in the water column.

[32] In the ventilated thermocline where the transport of δAr by advective processes is likely to be more important

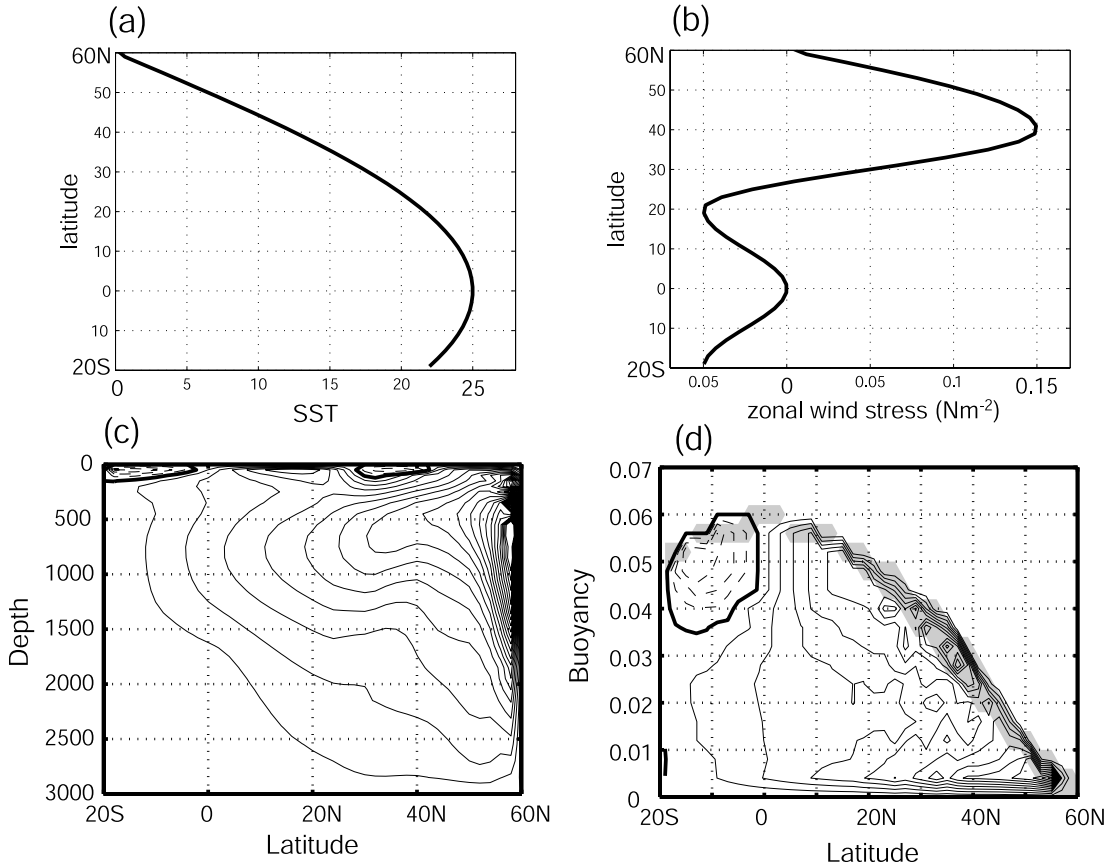

Figure 5. General Circulation Model surface boundary conditions for (a) temperature and (b) surface wind stress, and simulated meridional overturning circulation at steady state in (c) depth coordinates and (d) buoyancy coordinates.

than its redistribution by diffusion (the second and third term on the RHS of equation (21)), the rate of increase in δAr following a water parcel can be approximated by the SPR,

$$\frac{D\delta Ar}{Dt} \approx \left(\frac{\partial^2 Ar_{sat}}{\partial T^2}\right)\kappa\left(\frac{\partial T}{\partial z}\right)^2, \tag{22}$$

where $\frac{D}{Dt} = \frac{\partial}{\partial t} + \mathbf{u_{res}} \cdot \nabla$ is the Lagrangian derivative following the mean circulation. For typical magnitudes of $\kappa = 10^{-5}$ m^{2}s^{-1} and $\partial T/\partial z = 0.05$ deg m^{-1} in the subtropical thermocline, the theory predicts that argon saturation rises at the rate of 0.1% yr^{-1}. Thus argon saturation can rise on the order of a percent over the decadal timescale of thermocline ventilation, a signal that would be easily detected with current analytical methods. Thus the increase in δAr in a water parcel in the ocean interior may provide a powerful constraint on the diffusivity it experienced along its flow path.

[33] The dependence of SPR on diffusivity appears straightforward, but diapycnal diffusivity and thermocline stratification, both factors in SPR, are not necessarily independent of each other. Surface wind stress exerts the primary control over the depth of the ventilated thermocline [*Luyten et al.*, 1983], which is proportional to $\sqrt{w_{ek}}$ where w_{ek} is the rate of Ekman pumping. In this case, stratification is independent of diapycnal diffusivity, and SPR should scale linearly with the diapycnal diffusivity.

Ventilated thermocline

$$SPR \propto \kappa^{+1}. \tag{23}$$

[34] Below the wind-driven, ventilated thermocline, diffusion may play a more important role in setting the stratification. *Samelson and Vallis* [1997] suggested that the thickness of the ''internal thermocline,'' which is inversely proportional to its stratification, scales with $\sqrt{\kappa}$. Assuming that the surface temperature distribution is prescribed, the thermocline depth and stratification can be related via $\partial T/\partial z \propto \kappa^{-0.5}$. In this case, increased diffusivity reduces the stratification, leaving the SPR independent of diapycnal diffusivity.

Internal thermocline

$$SPR \sim constant. \tag{24}$$

[35] These results indicate that the sensitivity of ΔAr to diapycnal diffusivity may depend on which dynamical

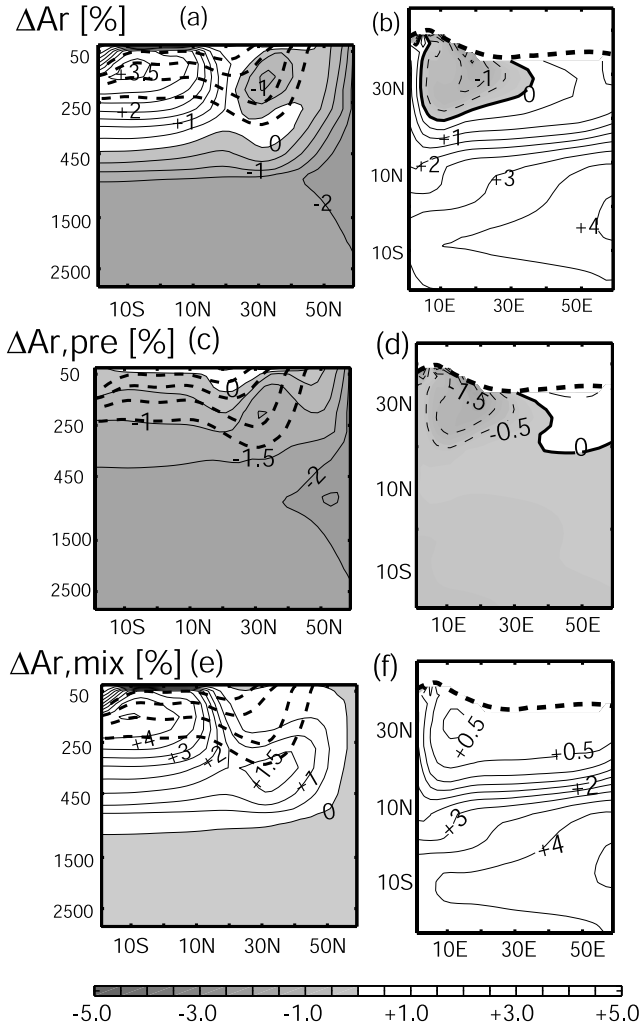

Figure 6. Simulated ΔAr distribution at steady state along (a) a meridional section at 30°E, and (b) the T = 15°C isopycnal surface. The depth scale is stretched for the top 500 m (Figure 6a). Dashed lines mark the position of isopycnals T = 18, 15, 12, 8°C from shallower to deeper depths (Figure 6a) and the outcrop of the 15°C isopycnal surface (Figure 6b). Shaded regions are undersaturated (ΔAr < 0). (c, d) Same as Figures 6a and 6b, but for ΔAr_{pre}. (e, f) Same as Figures 6a and 6b, but for ΔAr_{mix}.

balances maintain thermocline structure. It also implies that diapycnal diffusivity can be inferred from observed Ar distributions in the interior ocean by solving inverse problems based on the balance of equation (21) assuming steady state and adequate observations of Ar. In the following section, we explicitly simulate the argon distribution using an ocean general circulation model to evaluate these theoretical predictions.

3. Testing the Theory With an Ocean GCM

[36] We now wish to evaluate the degree to which the simple ideas developed in the context of the box model help us to understand the distribution and sensitivities of Ar in a more complicated, three-dimensional domain. To do this, we use the MIT Ocean General Circulation Model (GCM) [*Marshall et al.*, 1997a, 1997b] in which Ar is simulated as a passive tracer. Air-sea gas transfer is parameterized with a uniform mass transfer coefficient (piston velocity) of 2×10^{-5} m s^{-1}. Ar saturation is given by *Hamme and Emerson* [2004a], although model salinity is uniformly set to 35 psu.

3.1. Circulation and ΔAr

[37] The GCM is configured for a single hemispheric basin at coarse resolution (2 × 2 degrees, 30 vertical levels) similar to the model used by *Follows et al.* [2002]. The domain extends from 20°S to 60°N across 60 degrees of longitude, and is bounded by vertical walls and a flat bottom at 3000 m. The thickness of the vertical layers is 50 m for the top 5 layers, 100 m for the next 20 layers, and 150 m for the bottom 5 layers. Sea surface temperature (SST) is restored to a cosine profile with a timescale of 30 days (Figure 5a). Zonal wind stress is applied to the surface ocean as plotted in Figure 5b. For simplicity, there is no seasonal variation in the model.

[38] Modeled physical transport and tracer distributions are diagnosed once the model has reached a steady state (3000 years). Approximately 15 Sv of deep water is formed at high latitudes, and upwells at low and middle latitudes. When viewed in depth coordinates, the MOC appears dominated by the deep overturning circulation (Figure 5c); however, shallower wind-driven cells are clearly seen in the density coordinate (Figure 5d). Approximately 3 Sv of deep waters and 6 Sv of thermocline waters upwell between 20°S to 20°N.

[39] The distribution of ΔAr is shown for a meridional section and along an isopycnal surface (T = 15°C) in the thermocline in Figure 6. In the deep ocean, Ar is everywhere undersaturated by 1–2%. In the upper water column, Ar transitions from undersaturation in midlatitudes, to supersaturation in the tropics. The distribution of ΔAr in the thermocline (Figure 6b) shows that undersaturated

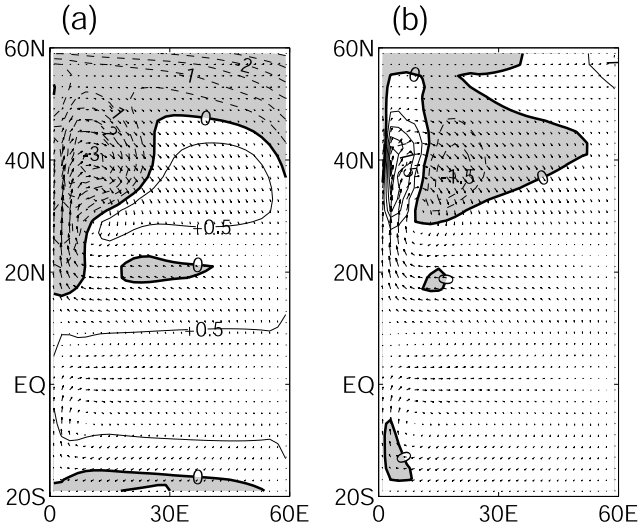

Figure 7. (a) Surface ΔAr distribution. (b) Difference between simulated ΔAr and predicted values based on simulated air-sea heat flux ($\Delta Ar^{(simulated)} - \Delta Ar^{(heat\ flux)}$).

waters are confined to the northwestern portion of the subtropical gyre, whereas the strongest supersaturations are found in the eastern tropics. In order to understand the mechanisms governing these patterns, we investigate the contribution of preformed ΔAr and its modification by mixing independently.

3.2. Air-Sea Heat Flux and Preformed ΔAr

[40] Because of the strong temperature dependence of Ar solubility, the air-sea flux of Ar is closely related to that of heat (Figure 7). In low latitudes, surface Ar is supersaturated and is fluxed out of the surface ocean (outgassing). At high latitudes, surface Ar is undersaturated owing to the heat loss and associated solubility increase, and Ar is fluxed into the surface ocean. Surface δAr computed from air-sea heat flux (equation (11)) is a good predictor of simulated δAr over most of the surface layer (Figure 6b).

[41] The largest difference between simulated δAr and that predicted by surface heat flux is found near the western boundary current which transports supersaturated water from the tropics to middle latitudes (e.g., 40°N, 5°E); making simulated ΔAr greater than the value predicted from local air-sea heat flux. The western boundary current separates from the coast, entering the interior gyre regions around (40°N, 20°E). Simulated ΔAr is smaller than the value predicted from air-sea heat flux there due to the horizontal advection of undersaturated water from upstream regions where strong heat loss occurs.

[42] Regions where total air-sea Ar flux differs from the thermally induced flux are associated with strong surface currents. In such regions, horizontal transport of δAr is locally important (see equation (21)). The length scale of the zonal dipole pattern described above can be obtained as a product of horizontal velocity and air-sea gas exchange timescale.

$$L_{dipole} \sim \frac{U\,h}{G}, \tag{25}$$

where U represents the velocity of horizontal current and h reflects the depth of the mixed layer. With a typical magnitudes of $U \sim 0.15$ m s^{-1}, $h \sim 100$ m, and $G = 2.0 \times 10^{-5}$ m s^{-1}, we find $L_{dipole} \sim 800$ km, consistent with the size of the simulated dipole pattern (Figure 7b).

[43] The pattern of surface Ar disequilibrium gets mapped into the ocean interior by physical transport processes, producing a three-dimensional distribution of preformed δAr. In order to isolate its contribution to the total δAr, we perform an additional simulation in which the solubility of Ar is linearized with temperature. In this ''linear-solubility'' experiment, diapycnal mixing cannot change Ar saturation in the interior ocean, so that $\Delta Ar_{mix} = 0$. In this case, modeled Ar saturation throughout the ocean is determined by the disequilibrium attained at the surface.

[44] The distribution of δAr derived from the linear solubility experiment (Figures 6c and 6d) is found to be everywhere negative, with the strongest undersaturations in the deep waters and in the ventilated thermocline. This can be understood in terms of the patterns of surface ΔAr. Although surface heating and cooling produce both supersaturations and undersaturations, only surface cooling is associated with water mass formation. Preformed ΔAr in the ocean interior therefore predominantly reflects the disequilibrium of waters undergoing heat loss. The contribution of preformed ΔAr can be seen to explain the regions of undersaturation found in the total ΔAr distribution (Figures 6a and 6b).

3.3. Mixing Component of ΔAr

[45] We now evaluate the contribution of diapycnal mixing to the Ar distribution. To isolate the role of diapycnal mixing, we perform a third experiment where the piston velocity is increased by a factor of 30, to 6×10^{-4} m s^{-1}. In this ''fast-gas exchange'' experiment, the surface waters are rapidly equilibrated so that the preformed ΔAr contribution is removed ($\Delta Ar_{pre} = 0$), and any Ar disequilibrium in the model is due to diapycnal mixing. In this case, we find that Ar is everywhere supersaturated, as expected (Figure 6). Significant supersaturations (>+0.5%) are confined to the upper water column shallower than 500 m, with highest values in the tropics and lowest values in the ventilated thermocline. In the subtropical thermocline (Figure 6f), we find a sharp gradient in ΔAr_{mix} between ventilated and unventilated regions indicating a stronger role for mixing in setting the stratification of the model's tropical thermocline, compared to the ventilated gyre.

[46] Simple theory predicts that the mixing component of thermocline Ar (ΔAr_{mix}) reflects the relative importance of vertical mixing and advective ventilation, and is linearly proportional to the mixing ratio of the low-latitude surface end-member, f_1 (equation (15)). Here we directly simulate the mixing ratio of low-latitude surface waters (f_1) using a dye tracer whose concentration is set to 1 at the surface south of 20°N and set to 0 elsewhere in the surface ocean. At steady state, the concentration of dye, which has been transported into the ocean interior, can be interpreted as the mixing ratio of the low-latitude surface end-member, f_1.

[47] On the isopycnal surface where $T = 15.0$°C, the mixing ratio of low-latitude surface waters is scarcely present in the newly ventilated waters in the subtropical thermocline north of 20°N, but becomes pervasive equatorward of 20°N (Figure 8a). This pattern is reminiscent of the ΔAr distribution on that surface. Indeed, ΔAr exhibits a strong linear correlation to f_1 (Figure 8b) away from the surface outcrop. The relationship between f_1 and ΔAr is due to the mixing component, ΔAr_{mix}, as simulated in the ''fast gas exchange'' experiment (Figure 8c), with little contribution from ΔAr_{pre} (Figure 8d). The correlation between f_1 and ΔAr is in excellent agreement with the simple three-end-member box model (equation (14)), assuming representative end-member temperatures of (T_1, T_2, T_3) = (22.5°C, 15.0°C, 1.0°C). These results confirm the theoretical prediction that the mixing component of Ar saturation is strongly correlated with the mixing ratio of low-latitude surface waters.

3.4. Separation of Preformed and Mixing Components

[48] The distributions of δAr derived from the ''fast-gas exchange'' experiment, and the ''linear-solubility'' experiment, provide independent estimates of the mixing and preformed components of ΔAr, respectively. We find that the distribution of ΔAr (Figure 6) is nearly identical to the

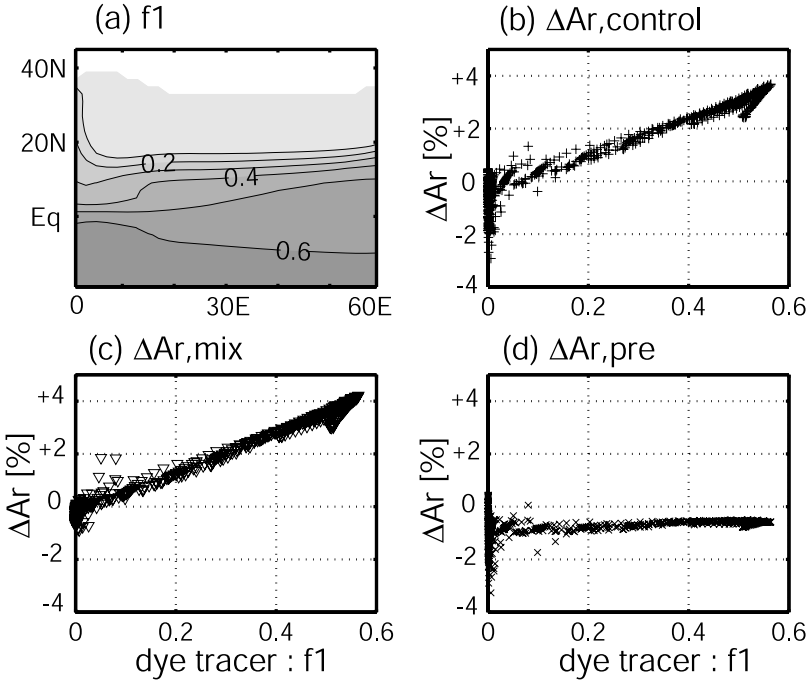

Figure 8. (a) Steady state distribution of dye tracer representing the mixing ratio of low-latitude surface waters, f_1, on T = 15°C surface. The relationship between the dye tracer and (b) ΔAr, (c) ΔAr_{mix}, and (d) ΔAr_{pre}, on the same isopycnal.

sum of these two independently derived components, $\Delta Ar_{mix} + \Delta Ar_{pre}$ (not shown), as suggested by the simple theory.

[49] As shown in the context of the box model, total ΔAr can also be separated into its mixing and preformed components, provided end-member Ar concentrations and temperatures are known (equation (18)). In the GCM, this also requires that thermocline waters can be characterized by only three end-members, so that only two independent conservative tracers, temperature and Ar, are sufficient to determine mixing ratios. We test the validity of this condition, to determine how well Ar observations in the real ocean might be able to distinguish the mixing and preformed components.

[50] We first estimate the temperature and Ar saturation of the surface end members. Low-latitude surface temperature is taken to be the average surface temperature equatorward of 20°N where f_1 is defined (T_1 = 22.5°C). T_2 is set to the temperature of the isopycnal of interest (15°C), and T_3 is equal to the model's deep ocean temperature (1°C). Ar saturations for the corresponding three end-members are ΔAr_1 = +0.5 (%), ΔAr_2 = 0 (%), and ΔAr_3 = −1 (%). Combining these estimates for the surface end-members and the isopycnal distribution of δAr, we can calculate the theoretical distribution of ΔAr_{mix}, following equations (17) and (18). Values of ΔAr_{mix} estimated in this way from distributions of temperature and Ar concentrations compare well to the mixing component explicitly simulated in the fast gas exchange experiment (Figure 9). The error is largest near the isopycnal outcrop, where δAr_{mix} is small (ΔAr_{mix} < 0.7 (%)), owing to high spatial variability in preformed ΔAr at the isopycnal outcrop.

3.5. Estimating Diapycnal Diffusivity

[51] We have argued that the Ar saturation in a water parcel transported primarily by advection will increase along its flow path at the saturation production rate (SPR) of $\left(\frac{\partial^2 Ar_{sat}}{\partial T^2}\right) \kappa \left(\frac{\partial T}{\partial z}\right)^2$ (equation (21)). Here we evaluate this prediction by computing the increase in δAr along

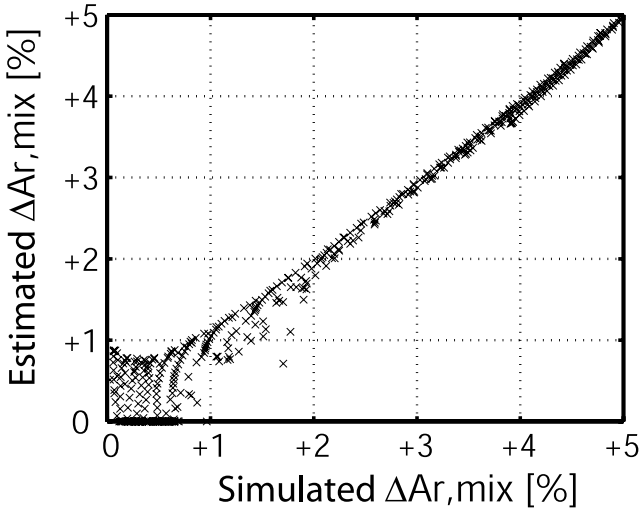

Figure 9. Relationship between ΔAr_{mix} simulated in the experiment with fast gas exchange and that estimated from the control run, applying the three-end-member mixing model to distinguish the mixing and preformed components of ΔAr (see equation (17)).

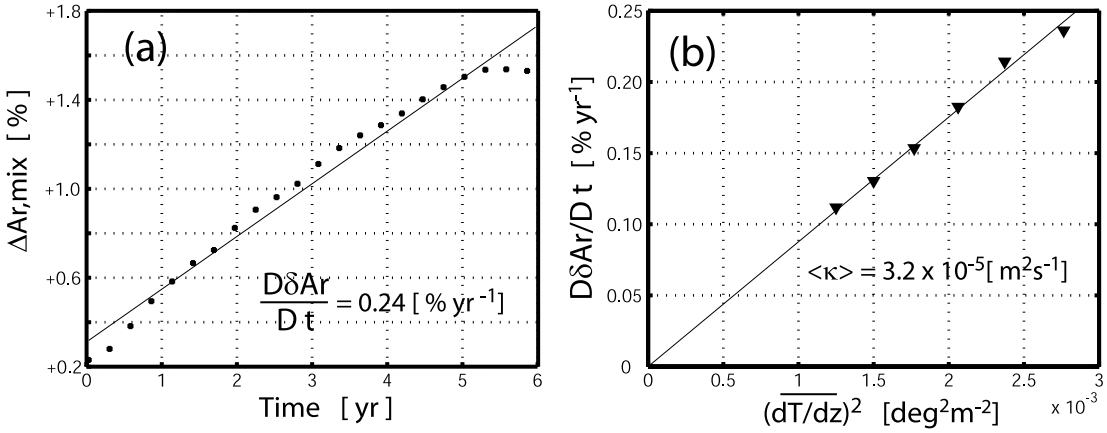

Figure 10. (a) Increase of ΔAr_{mix} following the trajectory of a water parcel which starts below the base of the mixed layer at 56°E and traverses the basin from west to east. (b) Relationship between SPR and the square of stratification from six trajectory calculations. The slope of this relationship is equal to the product of diapycnal diffusivity and the second derivative of the solubility curve.

Lagrangian trajectories from the midlatitude outcrop into the interior of the subtropical gyre. This increase provides a direct estimate of $\frac{D\delta Ar}{Dt}$, shown for one particular trajectory in Figure 10a, with a slope of approximately 0.24% yr^{-1}. The mean stratification along the trajectory of 0.052 deg m^{-1}, together with the curvature of Ar solubility implies an estimated diffusivity of 0.32×10^{-4} m^2 s^{-1}.

[52] Although diffusivity may be estimated from a single water parcel trajectory, several trajectories provide a more robust estimate (Figure 10b). We find that while $\frac{D\delta Ar}{Dt}$ varies significantly among different Lagrangian trajectories, it remains well correlated with the square of mean thermal stratification along each trajectory (Figure 10b). The average estimated diapycnal diffusivity of 0.32×10^{-4} m^2 s^{-1}, is remarkably close to the prescribed model diffusivity of 0.30×10^{-4} m^2 s^{-1}, and exhibits little variation among trajectories.

[53] Trajectory calculations based on δAr_{mix} values estimated directly from the total Ar and temperature distributions yield SPR values that are within 10% of those estimated from the δAr_{mix} values explicitly simulated in the fast gas exchange experiment. Since δAr_{mix} is not directly measurable and needs to be estimated from Ar and temperature distributions, this result suggests that Ar measurements can provide a useful constraint on the large-scale mean diapycnal diffusivity of the oceanic thermocline. In the following section, we further test these results in a series of sensitivity experiments in which diapycnal diffusivity and wind stress are varied over a wide range.

4. Sensitivity of ΔAr to Diapycnal Diffusivity

[54] The results so far have shown that diapycnal mixing plays an important role in the distribution of ΔAr. The mixing of waters across isopycnal surfaces has a direct effect of driving Ar concentrations toward supersaturation due to the nonlinearity of Ar solubility. In addition, preformed Ar disequilibrium is strongly influenced by air-sea heat fluxes. Air-sea heat fluxes are balanced by the large-scale transport of heat in the interior ocean which also depends on diapycnal diffusivity. Therefore both the preformed and mixing components of argon saturation are expected to depend on diapycnal diffusivity in the interior ocean. Furthermore, the two components of δAr are subject to redistribution due to the effect of mixing on the large-scale circulation. It is difficult to predict the net effect of these factors and we therefore investigate the sensitivity of δAr distributions to diapycnal diffusivity by performing model integrations in which κ is varied over a wide range.

[55] The changes in thermocline δAr that result from a threefold increase in diffusivity ($\kappa = 0.30 \times 10^{-4}$ m^2 s^{-1} to $\kappa = 1.0 \times 10^{-4}$ m^2 s^{-1}) are complex. Both increases and decreases in ΔAr are simulated over large regions (Figure 11a). Along the western boundary and in the western tropics, ΔAr increases by as much as 1.2% at higher κ. Increases are also found in the central part of the ventilated thermocline around (30°E, 20°N), albeit with reduced magnitude. In the unventilated region in the eastern tropics (south of 15°N), elevated diffusivity causes ΔAr to decrease as much as −0.4%, and similar decreases are found in a small region close the isopycnal outcrop in the western basin (15°E, 35°N).

[56] The opposing direction of changes in tropical versus subtropical δAr under elevated diffusivity (Figure 11a) reduces the background tropical-subtropical ΔAr gradient, which declines from supersaturated values in the tropics to undersaturated values in the subtropics (Figure 6). The opposing regional sensitivities of ΔAr to diffusivity suggests that the response in different regions is governed by different mechanisms. We therefore investigate the separate contributions of preformed and mixing disequilibria to the overall sensitivity of ΔAr to mixing.

4.1. Impact of Higher κ on ΔAr_{mix} and ΔAr_{pre}

[57] The impacts of increased mixing on ΔAr_{mix} and ΔAr_{pre} are easily determined by repeating the "linear

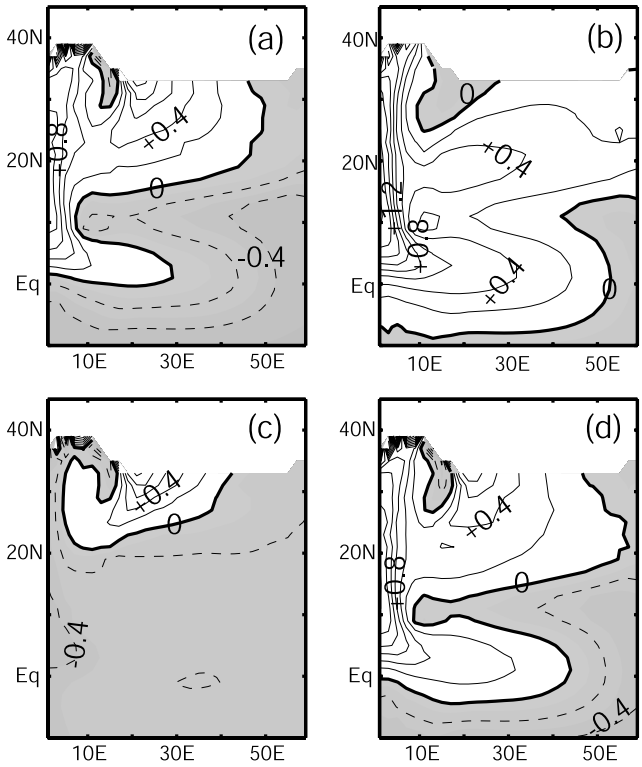

Figure 11. Difference in the saturation state of Ar on the T = 15°C surface between high mixing case (κ = 1.0×10^{-4} m^2 s^{-1}) and control run (κ = 0.3×10^{-4} m^2 s^{-1}) for (a) total Ar disequilibrium, ΔAr, (b) the mixing component only, ΔAr_{mix}, (c) the preformed component only, ΔAr_{pre}, and (d) the sum of Figures 11b and 11c. The total change in ΔAr due to enhanced diffusivity can be understood as the sum of separate and counteracting effects on preformed and mixing components of Ar disequilibrium. The contour interval is 0.2%.

solubility" and "fast gas exchange" experiments in the high-diffusivity model. As expected, ΔAr_{mix} generally increases with higher κ (Figure 11b), but with varying magnitudes. The sensitivity of ΔAr_{mix} is highest along the western boundary current. This is because the intensity of meridional overturning in the model is highly sensitive to the magnitude of κ, and the increased northward transport of tropical ΔAr_{mix} leads to a strong increase in ΔAr_{mix} along the western boundary. An increase in ΔAr_{mix} is also found in the ventilated thermocline. This change is attributable to the increased SPR in this region. In much of the subtropical thermocline, a high diapycnal diffusivity causes waters subducted into the interior to approach supersaturation more rapidly than in a less diffusive model, resulting in elevated supersaturations across much of the subtropics.

[58] In contrast, ΔAr_{pre} simulated in the linear solubility experiments generally decreases with higher κ (Figure 11c) in the tropics, as well as in the water mass formation region near the western boundary separation. As discussed in the box model theory, an increase in the vertical mixing rate drives a stronger meridional overturning circulation, and enhanced air-sea heat fluxes. Stronger cooling in regions of water mass formation at high latitudes leads to more undersaturated deep waters, and consequently for the low-latitude thermocline where deep waters upwell. In the GCM, enhanced heating occurs over the central basin at midlatitudes, which brings ΔAr toward supersaturation in much of the subtropical gyre. The spatially complex response of ΔAr to an increase in κ can now be understood as the sum of independent changes in the preformed and mixing components (Figure 11d), driven by changes in the intensity of air-sea heat fluxes, saturation production rate (SPR), and the physical mass transport.

[59] The dependence of SPR on diffusivity can now be compared with the limits predicted by the ventilated and internal thermocline theories (Table 2). We calculate the mean SPR between 25°N and 35°N on the isopycnal T = 15°C, taken to represent the ventilated thermocline, and T = 8°C, taken to represent the internal thermocline. For a tenfold increase in κ, SPR increases by a factor of $\sim$6 in the ventilated thermocline (T = 15°C). In a nearly adiabatic thermocline, κ would have little influence on the thermal stratification, and a tenfold increase in κ would yield a tenfold increase in SPR. The slightly smaller increase in SPR found here indicates that the impact of increased diffusivity does have some influence on mean stratification, leading to an SPR increase that is less than predicted by the theory. This is not surprising, given that the ventilated thermocline theory assumes no diffusivity, whereas the model has nonzero κ, even in the rapidly ventilated region of the thermocline.

[60] In the deeper thermocline (T = 8°C), SPR increases by only a factor of 2 for an order of magnitude increase in κ, where the internal thermocline theory would predict no increase in SPR. This shows that although increasing diffusivity does reduce stratification in the lower thermocline, it does not completely cancel the direct relationship between SPR and κ. Taken together, these results are qualitatively consistent with the theoretical prediction (equations (23) and (24)), in that SPR is sensitive to κ in the ventilated thermocline, but relatively insensitive to diffusivity in deeper waters, owing to the compensating effect of increased diffusivity on stratification.

4.2. Estimating Diapycnal Diffusivity of Sensitivity Experiments

[61] In order to test the ability of ΔAr distributions to provide a constraint on large-scale thermocline diffusivity, we use the method of Lagrangian trajectories (see section 3.5) across a suite of sensitivity experiments. We have

Table 2. Horizontally Averaged SPR From the Sensitivity Experiments for Isopycnal Surfaces T = 15°C and T = 8°C Taken to Represent the Ventilated and Internal Thermocline, Respectively[a]

Modeled κ	SPR (T = 8°C)	SPR (T = 15°C)
0.1	0.051	0.037
0.3	0.081	0.098
1.0	0.101	0.184

[a]Values for κ are in units of 10^{-4} m^2 s^{-1}. Values for SPR are in units of % yr^{-1}.

Table 3. Estimated κ Values From Sensitivity Experiments[a]

Prescribed κ	Wind Stress	Theoretically Estimated κ	STD
0.1	full	0.15	0.03
0.1	half	0.15	0.03
0.3	full	0.32	0.01
0.3	half	0.26	0.02
1.0	full	0.57	0.04
1.0	half	0.80	0.05

[a]Values for κ and its standard deviation (STD) are in units of 10^{-4} m^2 s^{-1}. For wind stress, "full" indicates the control forcing and "half" indicates that the intensity of the wind stress is reduced by half.

performed a series of model simulations in which diapycnal diffusivities are varied from 0.1×10^{-4} m^2 s^{-1} to 1.0×10^{-4} m^2 s^{-1} and the intensity of surface wind stress is varied by a factor of 2. In each experiment, we estimate the diapycnal diffusivity using equation (21) applied to six Lagrangian trajectories in the ventilated thermocline. The mean value and the standard deviation of estimated κ among the trajectories are reported in Table 3.

[62] Among all of the sensitivity experiments, we are able to recover the value of vertical diffusivity imposed in the model to within 50%, using only temperature and Ar values along flow trajectories along the subtropical thermocline. At intermediate values of diffusivity, the error in the estimated value of κ is considerably smaller (10–20%). In experiments with low diffusivity, the prescribed value of κ (0.1×10^{-4} m^2 s^{-1}) is overestimated by 50% for both high and low wind cases. We speculate that this error can be attributed to additional numerical mixing of tracers due to the model's finite differencing scheme. Argon may therefore be capturing the true effective diffusivity of the numerical model, which is higher than the explicitly prescribed diffusion coefficient.

[63] In contrast, in high diffusivity runs the Ar distribution underestimates κ by 20–40%. When diffusivity is large, thermocline structure may no longer be dominated by advective ventilation, in which case the quasi-adiabatic scaling of equation (22) is violated. That is, vertical diffusion acting on the δAr field (the second term of the RHS of equation (21)) will tend to erode the very δAr signal that it produces via the SPR. High diffusion will therefore attenuate the signal we are trying to estimate, leading to the underestimation of κ when diffusivity is large. Fortunately, neither of these biases in the estimation of model diffusivity are likely to be problematic when applied in the real ocean, where the artifact of numerical mixing does not exist, and where diffusivity is expected to be much lower than $\kappa = 1.0 \times 10^{-4}$ m^2 s^{-1}. We therefore expect that the systematic biases in this approach, although difficult to quantify, will be substantially less than 50%.

5. Conclusion and Summary

[64] Ongoing advances in the ability to accurately measure noble gas concentrations in the ocean [*Hamme and Emerson*, 2004b] offer a suite of conservative tracers with the potential to yield new insights into physical ocean processes underlying biogeochemical cycles. As observations begin to reveal basin-scale distributions of noble gases, especially Ar, a theoretical framework for interpreting such measurements in the context of large-scale ocean circulation will be required. We have presented a simple theory, summarized in Table 4, for understanding the distribution and sensitivity of Ar in terms of its two key governing processes, gas exchange and mixing.

[65] First, the incomplete equilibration of Ar between surface waters and the overlying atmosphere can produce both supersaturated and undersaturated concentrations. Surface disequilibria are mapped into the ocean interior along the pathways of ocean circulation, providing a preformed ΔAr distribution throughout the ocean. To the degree that the air-sea exchange of Ar is governed by air-sea heat flux, low-latitude surface waters will be supersaturated owing to heating of cold upwelled waters, and mid- and high-latitude surface waters will be undersaturated owing to ocean cooling. Preformed δAr in subsurface waters will preferentially reflect undersaturated conditions that prevail in regions of cooling, subduction and sinking.

[66] A second contribution to the δAr distribution arises however, in the presence of mixing across temperature surfaces. Because of the nonlinear dependence of Ar solubility on temperature, diapycnal mixing acts as an effective source of δAr, driving waters toward supersaturation. The deviation of δAr from its preformed value is a measure of the relative importance of mixing versus advection along the path of water mass transport. The saturation state of Ar in the ocean interior can thus generally be considered the sum of a negative (undersaturated) preformed value and a positive (supersaturated) contribution from the cumulative effect of mixing over the water mass history.

[67] These simple ideas provide a quantitative basis for understanding the Ar saturation state in different regimes of a three-dimensional model of ocean circulation (Table 4). In the ventilated thermocline of the northwestern subtropical gyre, where advective transport is rapid relative to vertical mixing, δAr remains near the preformed value obtained at the surface outcrop. Here δAr can be thought of as comprising a single end-member with little mixing-induced increase ("State 1" column in Table 4). In contrast, δAr values in the tropical thermocline ("State 2" column in Table 4) are well approximated by the supersaturated mixture of two end-members (cold deep water and warm surface water) suggesting that vertical mixing across isotherms is a dominant process setting the thermal structure. In much of the subtropics ("State 3" column in Table 4), between the extremes of the rapidly recirculating gyre in the northwest, and the shadow zone in the eastern tropics, the

Table 4. Summary of Ar Saturation State, its Controlling Mechanisms, and Sensitivities in Different Thermocline Regimes

Characteristic	Regime 1	Regime 2	Regime 3
Region	NW gyre	tropics	interior gyre
Typical ΔAr	$\Delta Ar < 0$	$\Delta Ar > 0$	$\Delta Ar \sim 0$
Component	ΔAr_{pre}	ΔAr_{mix}	$\Delta Ar_{pre} + \Delta Ar_{mix}$
Mechanism	ventilation	mixing	both
End-member	1	2	3
Sensitivity to κ	negative	negative	positive

saturation state of Ar has intermediate values, indicating a balance of ventilation and mixing.

[68] Our results suggest a sensitivity of Ar to mixing throughout the ocean, although the direction of that sensitivity is regionally different. In the deep ocean and the recirculating pool of the subtropical gyre, an increase in diapycnal diffusivity enhances cooling and the associated Ar undersaturation. In the western boundary current and in a broad swath of the subtropics, δAr increases owing to the direct effect of mixing on the production of supersaturations (SPR) there. In the tropical thermocline, where the effect of mixing governs δAr, increase in vertical diffusivity has little impact on the mixing component of δAr since the temperature contrast of the cold deep and warm surface end-members remain the same. The preformed δAr in the tropical thermocline, however, declines following the deep ocean, leading to an inverse relationship between diffusivity and δAr in the tropical thermocline, despite the importance of mixing.

[69] Because the sensitivity of δAr to diffusivity is dominated by the mixing effect in the subtropical thermocline, it is this region where Ar holds the greatest potential to constrain large scale ocean diffusivity. The rate at which δAr increases in a water parcel as a result of diapycnal mixing (SPR) is shown, from theoretical considerations, to scale with the product of diffusivity and the square of the stratification. The large-scale diffusivity of the ocean model can be successfully estimated from the rate of increase in δAr following a water parcel, with an accuracy that is better than 50% (see Table 3).

[70] This approach may be applied to observed ΔAr data if noble gases measurements are available from the outcrop of isopycnals to the interior subtropical gyre. Although Ar concentrations are unlikely to be measured directly along water parcel trajectories, we suggest that water mass ages derived from transient tracers such as CFCs could provide the means to estimate the rate of ΔAr increase with time. In addition, it may possible to improve the signal-to-noise ratio of such an approach, using multiple noble gases measurements whose solubilities have varying degrees of nonlinearity.

[71] The sensitivity of δAr to diapycnal diffusivity depends on the dynamical balances that maintain the stratification of the subtropical thermocline. In the ventilated thermocline, δAr is likely to scale linearly with diffusivity, while in the internal thermocline [*Samelson and Vallis*, 1997], the magnitude of δAr may be less sensitive to diffusion. In light of the different sensitivity regimes of Ar to diapycnal diffusivity, we suggest that once the oceanic distributions of Ar are empirically established, Ar may provide an important metric against which aspects of ocean circulation models can be evaluated.

[72] Observational constraints on the large-scale diffusivity of the oceanic thermocline have several implications for our understanding of the circulation and biogeochemical processes of the global ocean. First, the mixing of waters between the thermocline and abyss is one of the limiting factors for the uptake of anthropogenic CO_2. Because mixing in the interior ocean is much slower than air-sea exchange of CO_2, the current oceanic inventory of anthropogenic CO_2 is only about one third of the long-term potential [*Sabine et al.*, 2004]. Estimates of diapycnal mixing from noble gas measurements may improve models of future ocean CO_2 uptake. Second, the basic mechanisms by which nutrients are supplied to the surface ocean in low latitudes are still unresolved. Ultimately, diapycnal mixing must play an important role in sustaining low-latitude productivity, but it remains poorly quantified.

[73] Third, ocean mixing is not the only pathway by which cold abyssal waters are returned into the warm upper ocean. An alternative pathway for cold-to-warm water conversion involves the wind-driven upwelling in the Southern Ocean [*Toggweiler and Samuels*, 1993]. Our theory would predict that in such an adiabatic ocean, the mixing component of δAr would be much weaker than suggested by our numerical model, and the distribution of ΔAr would more closely resemble that of the linear solubility experiment. Finally, we note that ocean diffusivity may be spatially heterogeneous. For example, elevated diffusivity has been hypothesized in regions of tidally induced mixing over rough topography [*St. Laurent et al.*, 2002], where nutrient supply and anthropogenic CO_2 uptake might also be enhanced [*Sarmiento et al.*, 2004]. In principle, oceanic ΔAr distribution could help to identify such localized mixing "hot spots." We believe that a more complete picture of the distribution of ΔAr and potentially other noble gases will provide important avenues for addressing these outstanding questions.

Appendix A: Solution for ΔAr_{mix} in the Box Model Theory

[74] The two components of Ar saturation is not directly measurable from in situ observations. In the context of the box model theory, the partitioning between the two components can be determined if the mixing ratio of the end-members are determined as illustrated in equations (12) and (15).

[75] Here we assume that we know temperature, T_i, and Ar saturation, δAr_i of surface end-members and use them to constrain mixing ratios on the isopycnal $T = T_2$. Equation (8) shows that f_i are determined by a single parameter, γ, which is the relative strength of horizontal ventilation and vertical mixing. Equation (15) also shows the linear relationship between ΔAr_{mix} and f_1. Combining equations (8) and (15), we can express f_i in terms of δAr_{mix}.

$$f_1 = \frac{\delta Ar_{4,mix}}{a_2\,\Delta T_{12}\,\Delta T_{13}}, \tag{A1}$$

$$f_2 = 1 + \frac{\delta Ar_{4,mix}}{a_2\,\Delta T_{21}\,\Delta T_{23}}, \tag{A2}$$

$$f_3 = \frac{\delta Ar_{4,mix}}{a_2\,\Delta T_{31}\,\Delta T_{32}}. \tag{A3}$$

[76] Then we combine the expression for f_i of equations (A1)–(A3) with equations (12) and (17) to eliminate

$\delta Ar_{4,pre}$ to find the expression for $\delta Ar_{4,mix}$ in terms of directly measurable quantities (equation (18)).

Appendix B: ΔAr in a Continuously Stratified Ocean

[77] The governing equation for δAr can be derived from equations for Ar and T. We first multiply equation (19) by 2T, yielding

$$\frac{\partial T^2}{\partial t} + \mathbf{u}_{\text{res}} \cdot \nabla T^2 = \frac{\partial}{\partial z}\left(\kappa \frac{\partial T^2}{\partial z}\right) - 2\kappa\left(\frac{\partial T}{\partial z}\right)^2 + \frac{2T\mathcal{H}}{\rho\, c_p\, h}. \quad \text{(B1)}$$

Then we derive the equation for Ar_{sat} based on equation (2) by considering [$a_1 \times$ equation (19) + $a_2 \times$ equation (B1)].

$$\frac{\partial Ar_{sat}}{\partial t} + \mathbf{u}_{\text{res}} \cdot \nabla Ar_{sat} = \frac{\partial}{\partial z}\left(\kappa \frac{\partial Ar_{sat}}{\partial z}\right) - \left(\frac{\partial^2 Ar_{sat}}{\partial T^2}\right)\kappa\left(\frac{\partial T}{\partial z}\right)^2 + \left(\frac{\partial Ar_{sat}}{\partial T}\right)\frac{\mathcal{H}}{\rho\, c_p\, h}, \quad \text{(B2)}$$

where $\left(\frac{\partial Ar_{sat}}{\partial T}\right)$ is equal to ($a_1 + 2\ a_2\ T$) and $\left(\frac{\partial^2 Ar_{sat}}{\partial T^2}\right)$ is equal to ($2\ a_2$). Taking the difference between equations (20) and (B2) we find equation (21).

[78] **Acknowledgments.** We are thankful to Steve Emerson who motivated this work and provided stimulating discussions throughout its development. LuAnne Thompson, Ric Williams, and an anonymous reviewer provided useful comments for improving the manuscript. This publication is funded by the Program on Climate Change of the University of Washington and the Joint Institute for the Study of the Atmosphere and Ocean (JISAO) under NOAA Cooperative Agreement NA17RJ1232, contribution 1309.

References

Andrews, D., and M. McIntyre (1976), Planetary waves in horizontal and vertical shear: The generalized Eliassen-Palm relation and the zonal mean acceleration, *J. Atmos. Sci.*, *33*, 2031–2048.

Battle, M., M. Bender, M. Hendricks, D.T. Ho, R. Mika, G. McKinley, S. Fan, T. Blaine, and R. Keeling (2003), Measurements and models of the atmospheric Ar/N_2 ratio, *Geophys. Res. Lett.*, *30*(15), 1786, doi:10.1029/2003GL017411.

Bieri, R. H., M. Koide, and E. D. Goldberg (1966), The noble gas contents of Pacific seawaters, *J. Geophys. Res.*, *71*, 5243–5265.

Emerson, S., P. D. Quay, C. Stump, D. Wilbur, and R. Schudlich (1995), Chemical tracers of productivity and respiration in the subtropical Pacific Ocean, *J. Geophys. Res.*, *100*(C8), 15,873–15,888.

Emerson, S., C. Stump, D. Wilbur, and P. Quay (1999), Accurate measurement of O_2, N_2 and Ar gases in water and the solubility of N_2, *Mar. Chem.*, *64*, 337–347.

Follows, M., T. Ito, and J. Marotzke (2002), The wind-driven, subtropical gyres and the solubility pump of CO_2, *Global Biogeochem. Cycles*, *16*(4), 1113, doi:10.1029/2001GB001786.

Fuchs, G., W. Roether, and P. Schlosser (1987), Excess ^{3}He in the ocean surface layer, *J. Geophys. Res.*, *92*(C6), 6559–6568.

Hamme, R.C., and S.R. Emerson (2002), Mechanisms controlling the global oceanic distribution of the inert gases argon, nitrogen, and neon, *Geophys. Res. Lett.*, *29*(23), 2120, doi:10.1029/2002GL015273.

Hamme, R. C., and S. Emerson (2004a), The solubility of neon, nitrogen and argon in distilled water and seawater, *Deep Sea Res., Part I*, *51*(11), 1517–1528.

Hamme, R. C., and S. R. Emerson (2004b), Measurement of dissolved neon by isotope dilution using a quadrupole mass spectrometer, *Mar. Chem.*, *91*(1–4), 53–64.

Henning, C.C., D. Archer, and I. Fung (2006), Argon as a tracer of cross-isopycnal mixing in the thermocline, *J. Phys. Oceanogr.*, in press.

Ito, T., J. Marshall, and M. Follows (2004), What controls the uptake of transient tracers in the Southern Ocean?, *Global Biogeochem. Cycles*, *18*, GB2021, doi:10.1029/2003GB002103.

Keeling, R. (1993), On the role of large bubbles in air-sea gas exchange and supersaturation in the ocean, *J. Mar. Res.*, *51*, 237–271.

Luyten, J., J. Pedlosky, and H. Stommel (1983), The ventilated thermocline, *J. Phys. Oceanogr.*, *13*(2), 292–309.

Marshall, D. (1997), Subduction of water masses in an eddying ocean, *J. Mar. Res.*, *55*, 201–222.

Marshall, J., A. Adcroft, C. Hill, L. Perelman, and C. Heisey (1997a), A finite-volume, incompressible Navier Stokes model for studies of the ocean on parallel computers, *J. Geophys. Res.*, *102*(C3), 5753–5766.

Marshall, J., C. Hill, L. Perelman, and A. Adcroft (1997b), Hydrostatic, quasi-hydrostatic, and nonhydrostatic ocean modeling, *J. Geophys. Res.*, *102*(C3), 5733–5752.

Munk, W. (1966), Abyssal recipes, *Deep Sea Res.*, *13*, 207–230.

Sabine, C., et al. (2004), The oceanic sink for anthropogenic CO_2, *Science*, *305*(5682), 367–731.

Samelson, R., and G. Vallis (1997), Large-scale circulation with small diapycnal diffusion: The two-thermocline limit, *J. Mar. Res.*, *55*, 223–275.

Sarmiento, J. L., N. Gruber, M. Brzezinski, and J. P. Dunne (2004), High-latitude controls of thermocline nutrients and low latitude biological productivity, *Nature*, *427*, 56–60.

St. Laurent, L.C., H.L. Simmons, and S.R. Jayne (2002), Estimating tidally driven mixing in the deep ocean, *Geophys. Res. Lett.*, *29*(23), 2106, doi:10.1029/2002GL015633.

Toggweiler, J. R., and B. Samuels (1993), Is the magnitude of the deep outflow from the Atlantic Ocean actually governed by Southern Hemisphere winds?, in *The Global Carbon Cycle*, pp. 303–331, Springer, New York.

Warner, M. J., J. L. Bullister, D. P. Wisegarver, R. H. Gammon, and R. F. Weiss (1996), Basin-wide distributions of chlorofluorocarbons CFC-11 and CFC-12 in the North Pacific: 1985–1989, *J. Geophys. Res.*, *101*(C9), 20,525–20,542.

T. Ito, Joint Institute for the Study of the Atmosphere and Ocean, University of Washington, Box 354235, Seattle, WA 98195-4235, USA. (ito@atmos.washington.edu)

C. Deutsch, Program on Climate Change, School of Oceanography, University of Washington, Seattle, WA 98195, USA. (cdeutsch@ocean.washington.edu)